AD-A153 646 SUBSONIC AND TRANSONIC AERODYNAMICS OF A WRAPAROUND FIN CONFIGURATION(U) AIR FORCE ARMAMENT LAB EGLIN AFB FL R H WHITE ET AL. 15 JAN 85 AFATL-TR-85-22 1/1

UNCLASSIFIED F/G 20/4 NL

END

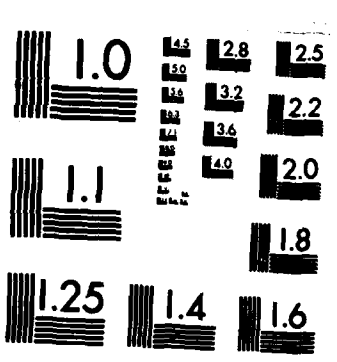

UNCLASSIFIED

SECURITY CLASSIFICATION OF THIS PAGE

AD-A153 646

1a. REPORT SECURITY CLASSIFICATION Unclassified/Public Release	1b. RESTRICTIVE MARKINGS Open Distribution
2a. SECURITY CLASSIFICATION AUTHORITY	3. DISTRIBUTION/AVAILABILITY OF REPORT Unlimited
2b. DECLASSIFICATION/DOWNGRADING SCHEDULE	
4. PERFORMING ORGANIZATION REPORT NUMBER(S)	5. MONITORING ORGANIZATION REPORT NUMBER(S) -TR-85-22 AFATL-~~85-TR-22~~
6a. NAME OF PERFORMING ORGANIZATION Air Force Armament Laboratory Aerodynamics Branch	6b. OFFICE SYMBOL (If applicable)
7a. NAME OF MONITORING ORGANIZATION AFATL/DLCA	
6c. ADDRESS (City, State and ZIP Code) Eglin AFB FL 32542-5000	7b. ADDRESS (City, State and ZIP Code)
8a. NAME OF FUNDING/SPONSORING ORGANIZATION	8b. OFFICE SYMBOL (If applicable)
9. PROCUREMENT INSTRUMENT IDENTIFICATION NUMBER A	
8c. ADDRESS (City, State and ZIP Code)	10. SOURCE OF FUNDING NOS.

PROGRAM ELEMENT NO.	PROJECT NO.	TASK NO.	WORK UNIT NO.
62602F	2567	02	42

11. TITLE (Include Security Classification)	
12. PERSONAL AUTHOR(S) R. H. White, R. S. Buff, W. H. Hathaway, G. L. Winchenbach	
13a. TYPE OF REPORT	13b. TIME COVERED FROM _____ TO _____
14. DATE OF REPORT (Yr., Mo., Day) 15 Jan 85	15. PAGE COUNT 10
16. SUPPLEMENTARY NOTATION	

17. COSATI CODES		
FIELD	GROUP	SUB. GR.

18. SUBJECT TERMS (Continue on reverse if necessary and identify by block number)
Subsonic, Aerodynamic Stability, Folding Fins, Transonic, Side Moment, Sub-munitions, WAF(Wraparound Fins), Pitch-Roll Resonance,

19. ABSTRACT (Continue on reverse if necessary and identify by block number)

Subsonic and transonic aerodynamic data for a wraparound fin configuration are presented. Free-flight aeroballistic tests to obtain these data were conducted at atmospheric pressure and over a Mach number range of 0.6 to 1.35. The aerodynamic coefficients and derivatives presented in this paper were extracted from the position-attitude-time histories of the experimentally measured trajectories using nonlinear numerical integration data reduction routines. Results of this analysis indicate that a dynamic instability exists above Mach 1.0 and is related to an out-of-plane side moment which is dependent on the pitch angle. The stability boundaries associated with this side moment are mapped. Designers should consider this moment whenever wraparound fins are used. Keywords include:

20. DISTRIBUTION/AVAILABILITY OF ABSTRACT UNCLASSIFIED/UNLIMITED ☒ SAME AS RPT. ☒ DTIC USERS ☐	21. ABSTRACT SECURITY CLASSIFICATION Unclassified
22a. NAME OF RESPONSIBLE INDIVIDUAL G. L. WINCHENBACH	22b. TELEPHONE NUMBER (Include Area Code) (904) 882-4085
	22c. OFFICE SYMBOL AFATL/DLCA

DD FORM 1473, 83 APR EDITION OF 1 JAN 73 IS OBSOLETE.

UNCLASSIFIED

SECURITY CLASSIFICATION OF THIS PAGE

DISCLAIMER NOTICE

THIS DOCUMENT IS BEST QUALITY PRACTICABLE. THE COPY FURNISHED TO DTIC CONTAINED A SIGNIFICANT NUMBER OF PAGES WHICH DO NOT REPRODUCE LEGIBLY.

SUBSONIC AND TRANSONIC AERODYNAMICS OF A WRAPAROUND FIN CONFIGURATION

Robert H. Whyte*
Advanced Munitions Engineer
Armament and Electrical Systems Department
General Electric Company
Burlington, Vermont

Lt. Randy S. Buff, USAF*
Aeroballistics Project Engineer
Aeromechanics Division
Air Force Armament Laboratory
Eglin Air Force Base, Florida

Wayne H. Hathaway*
Advanced Munitions Engineer
Armament and Electrical Systems Department
General Electric Company
Burlington, Vermont

G. L. Winchenbach*
Chief, Aeroballistics Section
Aeromechanics Division
Air Force Armament Laboratory
Eglin Air Force Base, Florida

* Member AIAA

Abstract

Subsonic and transonic aerodynamic data for a wraparound fin configuration are presented. Free-flight aeroballistic tests to obtain these data were conducted at atmospheric pressure and over a Mach number range of 0.6 to 1.35. The aerodynamic coefficients and derivatives presented in this paper were extracted from the position-attitude-time histories of the experimentally measured trajectories using nonlinear numerical integration data reduction routines. Results of this analysis indicate that a dynamic instability exists above Mach 1.0 and is related to an out-of-plane side moment which is dependent on the pitch angle. The stability boundaries associated with this side moment are mapped. Designers should consider this moment whenever wraparound fins are used.

Nomenclature

A	reference area, $\pi d^2/4$
a_c	Coriolis acceleration
AF	amplication factor
C_ℓ	roll moment coefficient, ℓ/qAd
$C_{\ell p}$	slope of the roll moment vs spin
$C_{\ell\gamma\alpha 2}$	induced roll moment derivative
C_m	pitching moment coefficient, m/qAd
C_{mq}	pitch damping derivative, $\frac{\partial C_m}{\partial \left(\frac{qd}{2V}\right)}$
C_{mq2}	quadratic pitch damping coefficient
$C_{m\alpha}$	slope of pitching moment vs α
$C_{m\alpha 3}$, $C_{m\alpha 5}$	cubic and fifth order pitching moment coefficients
$C_{m_{\alpha_M}}$	slope of pitching moment derivative vs Mach number
C_N	normal force coefficient, F_N/qA
$C_{N\alpha}$	slope of the normal force vs α
$C_{N\alpha 3}$, $C_{N\alpha 5}$	cubic and fifth order normal force coefficient
C_n	side moment coefficient, n/qAd
$C_{n\alpha}$	slope of side moment vs α
$C_{np\alpha}$	Magnus moment derivative
C_X	axial force coefficient, axial force/qA
C_{X_0}	axial force coefficient at zero angle of attack
C_{X_M}	slope of axial force coefficient vs Mach number
d	body diameter and reference length
g	acceleration due to gravity
I_x, I_y	moments of inertia about the x and y axis
K_{10}, K_{20}	magnitude of linear theory vectors
K_T	magnitude of trim vector
L	model length
ℓ, m, n	roll, pitch, and yaw moments
$\bar{m}$	model mass
M	Mach number
p, q, r	rolling, pitching, and yawing velocities
$\bar{q}$	dynamic pressure
R_{e_L}	Reynolds number based on model length
u, v, w	velocities in the X, Y, Z direction

Nomenclature — Continued

X, Y, Z	fixed plane coordinates
V	total velocity
α	total angle of attack
α_M	maximum total angle of attack
γ	aerodynamic roll angle
θ, ψ, ϕ	rotation angles
ω_{10}, ω_{20}	linear theory vector frequencies
$\omega'_{10}, \omega'_{20}$	change in linear theory vector frequencies with distance
$\lambda_{10}, \lambda_{20}$	linear theory vector damping rates
$\overline{\delta^2}$	effective angle of attack squared
Superscripts	
$(\cdot)$	first derivative with respect to time
$(-)$	total values

Introduction

The test results discussed in this paper were obtained in the Aeroballistic Research Facility (ARF) of the Air Force Armament Laboratory. The primary purpose of the tests was to obtain the aerodynamic coefficients and derivatives of the subscale model such that trajectory histories of the full scale item could be predicted. The models were of the Wraparound Fin (WAF) design. Because of packaging advantages, designers of tube-launched and dispenser-launched submunitions have used WAF designs for years[1-3]. These designs permit the fins to be neatly folded around the body prior to launch. This saves valuable space and allows either the maximum number or size of submunitions to be packaged in the dispenser or tube. Upon launch the fins are deployed to provide the required aerodynamic stability during flight. However, many of these past designs have experienced unusual and adverse flight dynamics[4]. Many of these problems were thought to be related to the erratic rolling motion of the munition caused by the WAF design[5-6]. During the test program it was observed that some of the models displayed unusual damping characteristics (generally unfavorable). The analysis of the experimentally measured motion profiles indicated that these unfavorable damping characteristics were caused by the existence of an out-of-plane (side) moment due to pitch angle.

The purpose of this paper is to describe these free-flight aerodynamic tests, present the data obtained, and discuss the ramifications of the out-of-plane moment. The stability boundaries of this side moment are developed and indicate that this configuration is dynamically stable subsonically and unstable supersonically. It is suspected that this side moment is symptomatic of WAF configurations and should be of particular concern to the designer.

Facilities, Models, and Test Conditions

Free Flight Range

The free flight tests were conducted in the ARF[7] which is part of the Air Force Armament Laboratory, Eglin Air Force Base, Florida. This facility is an enclosed, atmospheric, instrumented, concrete structure used to examine the exterior ballistics of various free flight configurations. The facility contains a gun room, control room, model measurement room, blast chamber, and the instrumented range.

The 207-meter instrumented length of the range has a 3.66-meter-square cross section for the first 69 meters and a 4.88-meter-square cross section for the remaining length. The range has 131 locations available as instrumentation sites. Each location has a physical separation of 1.52 meters, and presently 50 of the sites are used to house fully instrumented orthogonal shadowgraph stations. The maximum shadowgraph window, an imaginary circle in which a projectile in flight will cast a shadow on both reflective screens, is 2.13 meters in diameter. A laser-lighted photographic station is located in the uprange end of the instrumented range. This photographic station yields four orthogonal photographs, permitting a complete 360-degree view of the projectile as it passes the station on its downrange trajectory. Also, a direct shadowgraph station, consisting of a spark gap and film holder, is located in the uprange end of the range. Since the film is illuminated directly by the spark as the model passes the station, high quality flow field photographs are obtained. The nominal operating temperature of the range is 22 degrees Celsius.

Models and Test Conditions

The overall model geometry and WAF details are shown in the sketches of Figure 1. Fourteen of these models were flown in the facility during the test program, eleven models were successfully analyzed, and aerodynamic coefficients and derivatives extracted. The tests were conducted at atmospheric pressure and over a Mach number range of 0.58 to 1.35. The measured physical properties of each of the models and the associated test conditions for each of the eleven flights successfully analyzed are presented in Table 1.

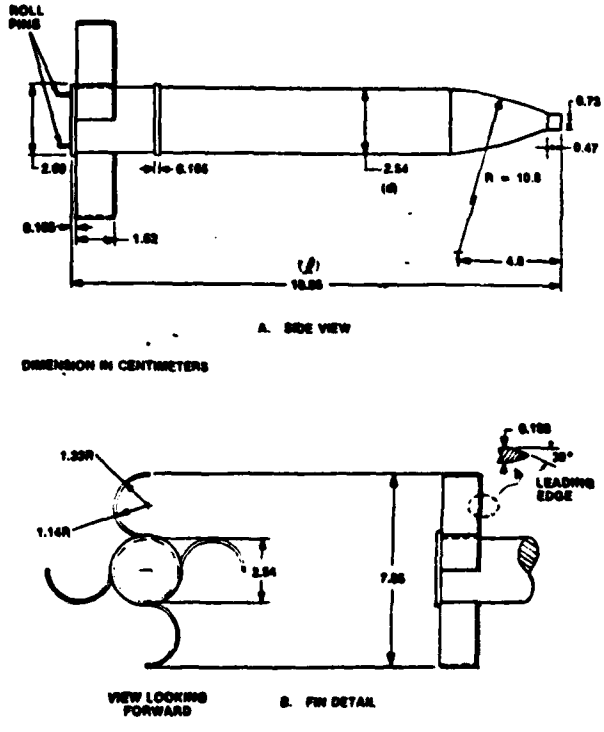

Figure 1. Model Configuration

Table 1. PHYSICAL MEASUREMENTS AND TEST CONDITIONS

Shot No.	Mach Number	$R_{e_L} \cdot 10^6$	$\bar{\delta}^2$ (deg)	d Model Diameter (cm)	L Model Length (cm)	$\bar{m}$ Model Mass (gm)	I_x (gm cm^2)	I_y (gm cm^2)	X_{cg} / L*
71	0.579	2.47	15.3	2.529	18.930	215.71	256.0	7273.	0.4820
72	0.586	2.52	3.9	2.539	18.945	216.47	259.1	7514.	0.4832
73	0.588	2.52	6.4	2.539	18.942	216.39	255.8	7345.	0.4845
74	0.722	3.11	9.9	2.522	18.933	214.11	254.8	7329.	0.4829
77	0.760	3.28	0.3	2.521	18.939	215.59	255.3	7435.	0.4811
75	0.773	3.31	0.6	2.524	18.943	220.76	256.6	7734.	0.4831
76	0.783	3.39	0.0	2.522	18.950	214.44	256.1	7318.	0.4826
81	1.028	4.44	28.4	2.520	18.963	216.64	256.6	7654.	0.4851
82	1.092	4.69	2.6	2.540	18.942	216.42	256.7	7382.	0.4814
87	1.243	5.40	72.6	2.538	18.962	216.16	256.1	7711.	0.4836
88	1.353	5.80	10.0	2.540	18.937	215.43	256.4	7588.	0.4835

* $X_{cg/\ell}$ Measured from the nose

The models were launched from a 152-mm, inside diameter, smooth bore compressed gas launcher using a conventional four-piece sabot. No attempt was made to augment the initial angular disturbances of the models as the model/sabot package exited the launcher. The angular disturbances that were obtained were caused by the normal sabot separation process. A photograph of the model/sabot package is shown in Figure 2, and a typical flow field photograph of a model in supersonic flight is shown in Figure 3.

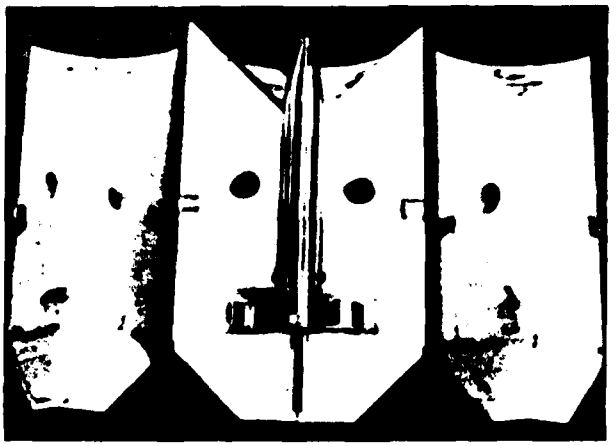

Figure 2. Model/Sabot Package

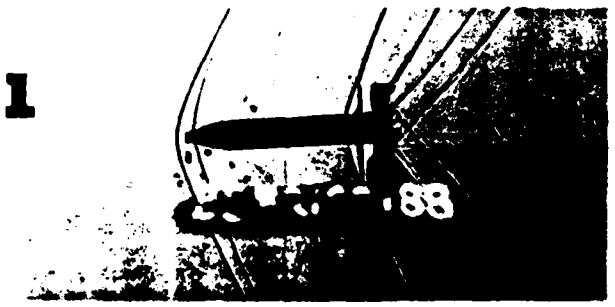

Figure 3. Flow Field Photograph (Shot 88, M = 1.353)

Free Flight Data Reduction

Extraction of the coefficients and derivatives is the primary goal in analyzing the trajectories measured in the ARF. This is accomplished by using the Aeroballistic Research Facility Data Analysis System (ARFDAS)[8] shown in Figure 4. ARFDAS incorporates a standard linear theory analysis[9-10] and a six-degree-of-freedom (6DOF) numerical integration technique. The 6DOF routine incorporates the Maximum Likelihood Method (MLM) to match the theoretical trajectory to the experimentally measured trajectory. The MLM is an iterative procedure which adjusts the aerodynamic coefficients to maximize a likelihood function. The application of this likelihood function eliminates the inherent assumption in least squares theory that the magnitude of the measurement noise must be consistent between dynamic parameters (irrespective of units). In general, the aerodynamics can be nonlinear functions of the angle of attack, Mach number, and aerodynamic roll angle.

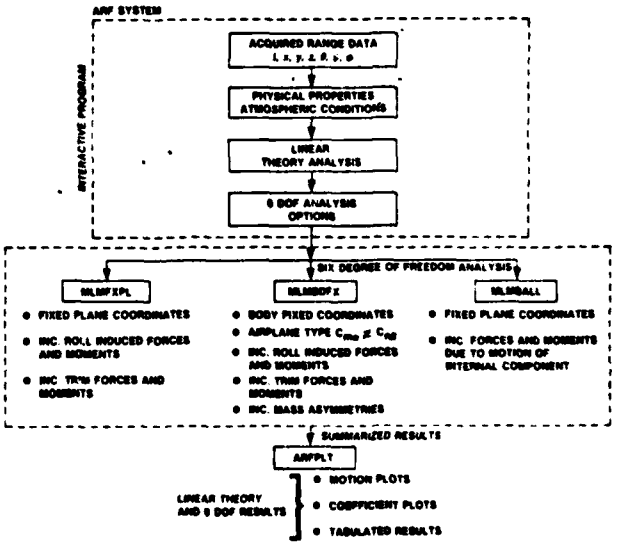

Figure 4. Data Analysis System — Aeroballistic Research Facility

ARFDAS, Figure 4, represents a complete ballistic range data reduction system capable of analyzing both symmetric and unsymmetric bodies.[11] The essential steps of the data reduction system are to (1) assemble the basic dynamic range data (time, position, angles), physical properties of the models, and atmospheric conditions existing in the facility at the time of testing, (2) perform a linear theory analysis, and (3) perform a 6DOF analysis. These steps have been integrated into ARFDAS to provide the test engineer with a convenient and efficient means of interaction. At each step in the analysis, permanent records for each shot are maintained such that subsequent analyses exercising various options are much faster.

The flight of each model fired in the ARF was initially analyzed separately, then the flights at similar Mach numbers were simultaneously analyzed using the 6DOF multiple fit technique. This provides a common set of aerodynamics that matched each of the separately measured position-attitude-time profiles. The multiple fit approach provides a more complete range of angle of attack and roll orientation combinations than would be available from any one flight considered separately. This increases the probability that the determined coefficients define the model's aerodynamics over the entire range of trajectories.

Equations of Motion

The aerodynamic data presented in this paper were obtained using the fixed plane 6DOF analysis (MLMFXPL). The equations of motion are derived with respect to a fixed plane coordinate system. The x-axis points downrange, the y-axis points to the left looking downrange, and the z-axis points up. The 6DOF differential equations of motion in this system are:

$$\dot{u} = g \sin\theta - qw + rv - a_{cu} + F_{x/\bar{m}} \tag{1}$$

$$\dot{v} = -ru - rw \tan\theta - a_{cv} + F_{y/\bar{m}} \tag{2}$$

$$\dot{w} = -g \cos\theta + rv \tan\theta + qu - a_{cw} + F_{z/\bar{m}} \tag{3}$$

and

$$\dot{p} = \ell/I_x \tag{4}$$

$$\dot{q} = -r^2 \tan\theta - I_x/I_y\, rp + m/I_y \tag{5}$$

$$\dot{r} = qr \tan\theta + I_x/I_y\, qp + n/I_y \tag{6}$$

Once the definition of the forces and moments are made, the solution of equations (1-6) will define the 6DOF flight motion of a symmetric missile in fixed plane coordinates. Since the position-attitude measurements, as required from a ballistic spark range, are obtained with respect to an earth-fixed axis system, additional transformation equations are required. These transformation equations are shown below in terms of the fixed plane Euler angles (θ, ψ) and the angle of rotation about the missile axis (ϕ).

$$\dot{x} = u \cos\theta \cos\psi - v \sin\psi + w \sin\theta \cos\psi \tag{7}$$

$$\dot{y} = u \cos\theta \sin\psi + v \cos\psi + w \sin\theta \sin\psi \tag{8}$$

$$\dot{z} = -u \sin\theta + w \cos\theta \tag{9}$$

$$\dot{\theta} = q \tag{10}$$

$$\dot{\psi} = r/\cos\theta \tag{11}$$

$$\dot{\phi} = p + r \tan\theta \tag{12}$$

Coriolis accelerations (a_{cu}, a_{cv}, a_{cw}) are also included in equations (1-3). The preceding equations (1-12) are numerically integrated using a fourth-order Runge-Kutta scheme.

Aerodynamic Model

Initially, considerable difficulty was encountered in attempting to fit the experimentally measured trajectories associated with this WAF configuration. Various combinations of nonlinearities and roll dependencies were assumed; however, these fits failed to adequately match the experimentally measured motion patterns. It was suspected that the wraparound fins were causing a side moment due to pitch ($C_{n\alpha}$). This out-of-plane moment was therefore added to the definition of the associated moment equations and the fits reaccomplished. These fits successfully matched the solutions of the theoretical equations of motion to the experimentally measured motion patterns, indicating that this side moment due to pitch angle was present for this WAF configuration. The basic definitions of the aerodynamic forces and moments (including the $C_{n\alpha}$ term), as used in obtaining the results reported herein, are shown below:

$$F_x = -\bar{q}AC_x \tag{13}$$

$$F_y = \bar{q}A\left[-\bar{C}_{N\alpha}\frac{v}{V} + \frac{pd}{2V}\bar{C}_{Yp\alpha}\frac{w}{V} + \bar{C}_{Y\gamma\alpha}\frac{w}{V} + \bar{C}_{N\delta}\,\delta_A \sin\phi - \bar{C}_{N\delta}\,\delta_B \cos\phi\right] \tag{14}$$

$$F_z = \bar{q}A\left[-\bar{C}_{N\alpha}\frac{w}{V} - \frac{pd}{2V}\bar{C}_{Yp\alpha}\frac{v}{V} - \bar{C}_{Y\gamma\alpha}\frac{v}{V} - \bar{C}_{N\delta}\,\delta_A \cos\phi - \bar{C}_{N\delta}\,\delta_B \sin\phi\right] \tag{15}$$

$$\ell = qAd\left[\frac{pd}{2V}\bar{C}_{\ell p} + \bar{C}_{\ell}\right] \tag{16}$$

$$m = \bar{q}Ad\left[\bar{C}_{m\alpha}\frac{w}{V} + \frac{qd}{2V}\bar{C}_{mq} + \frac{pd}{2V}\bar{C}_{np\alpha}\frac{v}{V} + \bar{C}_{n\gamma\alpha}\frac{v}{V} + \bar{C}_{n\alpha}\frac{v}{V} + \bar{C}_{m\delta}\,\delta_A \cos\phi - \bar{C}_{m\delta}\,\delta_B \sin\phi\right] \tag{17}$$

$$n = \bar{q}Ad\left[-\bar{C}_{m\alpha}\frac{v}{V} + \frac{rd}{2V}\bar{C}_{mq} + \frac{pd}{2V}\bar{C}_{np\alpha}\frac{w}{V} + \bar{C}_{n\gamma\alpha}\frac{w}{V} + \bar{C}_{n\alpha}\frac{w}{V} + \bar{C}_{m\delta}\,\delta_A \sin\phi + \bar{C}_{m\delta}\,\delta_B \cos\phi\right] \tag{18}$$

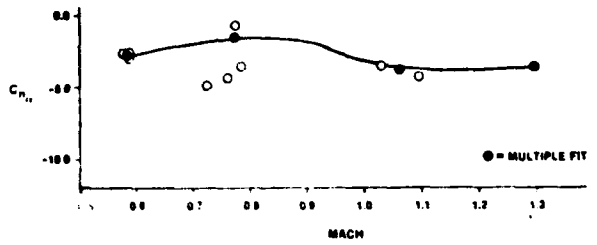

Figure 10. Side Moment Derivative

Some of the models also displayed unusual roll characteristics; for example, the models tended to roll clockwise subsonically and counterclockwise supersonically. In the transonic region, roll reversals occurred on some flights. The roll profiles obtained from the various flights are shown in Figure 12 along with the theoretical fits. Generally, the theoretical roll profiles matched the measured roll profiles reasonably well; nevertheless, the analysis routine had difficulty in determining the roll damping derivative, (C_{lp}), as is evident from the values listed in Table 2.

A cursory review of the data shown in Figures 5 through 10 and Table 2 would not indicate any potential dynamic problems associated with this configuration. However, the models flown at supersonic velocities developed an increasing angle of attack history during their downrange trajectories, indicating a dynamic instability at the supersonic conditions. Typical angular motion plots for a subsonic, transonic, and supersonic flight are shown in Figure 11 to illustrate this dynamic instability. Also notice the tendency of the motion patterns to become circular independent of whether the motion grows or damps.

Although all the aerodynamic coefficients and derivatives presented in Figures 5 through 10 and tabulated in Table 2 were obtained using the 6DOF analysis techniques, linear theory fit parameters such as vector magnitudes, vector frequencies, and damping rates are also shown in Table 3. When viewing these results, it should be remembered that the nutation vector can be either K_1 or K_2 depending on the direction of spin (p). By definition, the nutational vector rotates in the same direction as spin. For example, if the spin rate is negative, the nutation vector would be the one that has a negative frequency (ω_{20}).

Table 2. 6DOF MULTIPLE FIT RESULTS

Shot Number	Mach No.	δ^2 α_{max}	C_{x0} $C_{x\alpha 2}$ $C_{x\alpha 4}$	$C_{N\alpha}$ $C_{N\alpha 3}$ $C_{N\alpha 5}$	$C_{Yp\alpha}$ $C_{np\alpha}$ $C_{np\alpha 3}$	$C_{m\alpha}$ $C_{m\alpha 3}$ $C_{m\alpha 5}$	C_{mq} C_{mq2} C_{mq4}	$C_{Z\gamma\alpha 3}$ $C_{m\gamma\alpha 3}$ $C_{m\gamma\alpha}$	$C_{Y\gamma\alpha 3}$ $C_{n\gamma\alpha 3}$ $C_{n\gamma\alpha}$	$C_{\varrho\gamma\alpha 2}$ $C_{x\gamma\alpha 2}$ $C_{\varrho p}$	C_{xm} $C_{m\alpha m}$ $C_{n\alpha}$	PE-X PE-YZ	PE-θ, ψ PE-σ
71,72,73	0.585	8.6	0.759	14.03	0.00	-46.249	-288.1	0.0	0.0	0.00	0.20	0.0020	0.098
		7.6	2.000	0.00	0.00	785.040	0.0	0.0	0.0	0.00	0.00	0.0003	1.193
			0.0	0.0	0.0	0.0	0.0	0.0	0.0	-22.385	-2.85		
75,76,77	0.773	0.3	0.792	15.00	0.00	-52.045	-300.0	0.0	0.0	0.00	0.00	0.0012	0.135
		2.9	2.000	9.00	0.00	0.000	0.0	0.0	0.0	0.00	0.00	0.0013	2.620
			0.0	0.0	0.0	0.0	0.0	0.0	0.0	-3.473	-1.56		
81,82	1.062	15.2	1.420	14.63	0.00	-41.192	-290.9	0.0	0.0	0.00	-0.40	0.0008	0.193
		7.5	7.243	0.00	0.00	-223.010	0.0	0.0	0.0	0.00	62.11	0.0007	30.280
			0.0	0.0	0.0	0.0	0.0	0.0	0.0	-27.990	-3.74		
87,88	1.296	40.8	1.379	14.01	0.00	-32.549	-200.0	0.0	0.0	0.00	-0.20	0.0028	0.406
		12.1	4.036	0.00	0.00	-143.530	0.0	6.6	21.9	0.00	0.00	0.0007	29.710
			0.0	0.0	0.0	1163.7	0.0	0.0	0.0	-5.000	-3.57		

Table 3. LINEAR THEORY FIT PARAMETERS

Shot No.	Mach.	δ^2 DEG2	K10 DEG	K20 DEG	λ_1 1/M	λ_2 1/M	ω_{10} DEG/M	ω_{20} DEG/M	ω_1' DEG/M	ω_2' DEG/M	K_T DEG	p DEG/M	p/ω_N
71	0.579	15.3	3.34	4.21	-0.04871	-0.00560	37.235	-36.373	-0.97954	-0.04040	0.00	10.93	0.29
72	0.586	3.9	3.40	1.64	-0.04858	-0.00842	38.022	-36.972	0.06226	-0.06083	0.00	11.39	0.30
73	0.588	6.4	2.57	2.74	-0.05107	-0.00730	36.702	-38.460	0.10714	-0.01966	0.00	0.98	0.03
74	0.722	9.9	1.34	4.47	-0.04094	-0.01196	54.777	-36.167	-0.43364	-0.08876	0.00	-1.58	0.04
77	0.760	0.3	0.63	0.67	-0.02850	-0.00695	40.339	-41.013	-0.00791	-0.01819	0.00	8.85	0.22
75	0.773	0.6	0.67	1.46	-0.03640	-0.02280	42.704	-39.711	-0.14725	-0.02454	0.00	-1.09	0.03
76	0.783	0.0	0.17	0.18	-0.02625	-0.02297	42.651	-39.862	0.00000	0.00000	0.00	19.08	0.45
81	1.028	28.4	2.94	5.17	-0.04990	0.00007	35.362	-36.848	0.07480	-0.05809	0.00	-1.81	0.05
82	1.092	2.6	0.21	1.18	-0.02998	0.00650	32.199	-34.843	0.09224	-0.04981	0.00	-14.16	0.41
87	1.243	72.6	0.80	4.82	-0.01410	0.00976	35.625	-33.690	-0.14056	-0.01799	0.00	-36.11	1.07
88	1.353	10.0	0.30	3.20	-0.01312	-0.00067	35.761	-32.725	0.00000	-0.04725	0.00	-29.91	0.91

The aerodynamic coefficients and derivatives, shown in equations (13-18), were expanded as functions of Mach number, sine of the total angle of attack, and the aerodynamic roll angle. These expansions are shown in detail in reference 8. However, the side moment expansion was assumed to be linear, or $\bar{C}_n = C_n$ (thus $\bar{C}_{n\alpha} = C_{n\alpha}$).

Results

The aerodynamic coefficients and derivatives extracted from the experimentally measured trajectories are plotted in Figures 5 through 10 and tabulated in Table 2. These figures show the zero angle-of-attack coefficients and derivatives obtained using the fixed plane 6DOF analysis. The nonlinear terms obtained from the present analysis are shown in Table 2 and were derived using the multiple fit technique only. The multiple fit results would be expected to be superior to the analyses of the individual flights for the reasons previously discussed. However, some of the values obtained from the individual flights are plotted in Figures 5 through 10 because they assist in showing the various trends in the data.

Briefly the data shown in these figures indicate that:

1. The subsonic drag coefficient is about 0.75 and increases to about 1.4 supersonically (refer to Figure 5).

2. The normal force derivative is about 14 (refer to Figure 6).

3. The models are statically stable with a large static margin of about 30 to 45 percent of the body length (refer to Figures 7 and 9).

4. The damping-in-pitch derivatives vary between -300 and -200 (refer to Figure 8).

5. The side moment derivative (due to pitch) that was added to the reduction routine was determined to be about -3.0 (refer to Figure 10).

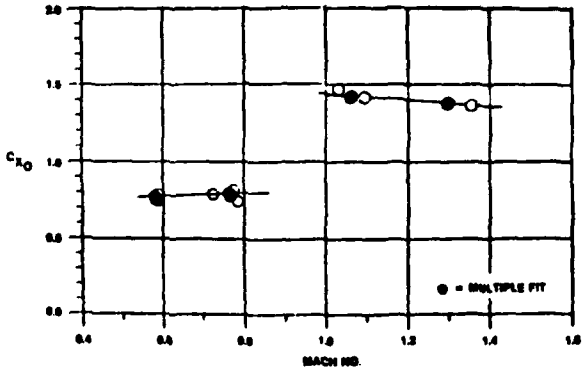

Figure 5. Axial Force Coefficient

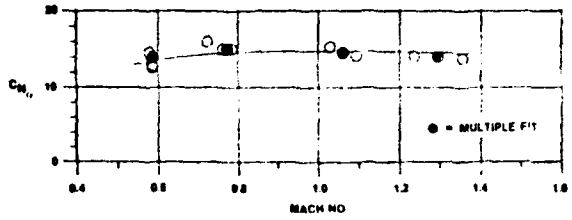

Figure 6. Normal Force Derivative

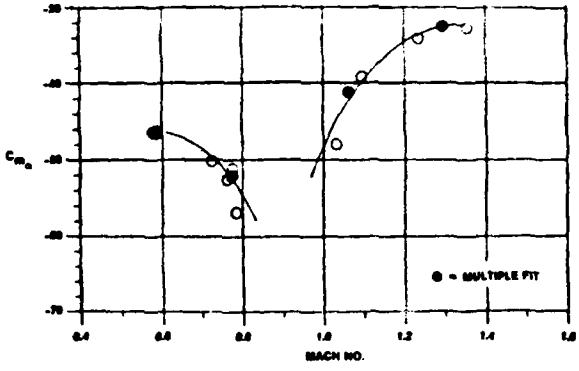

Figure 7. Pitching Moment Derivative

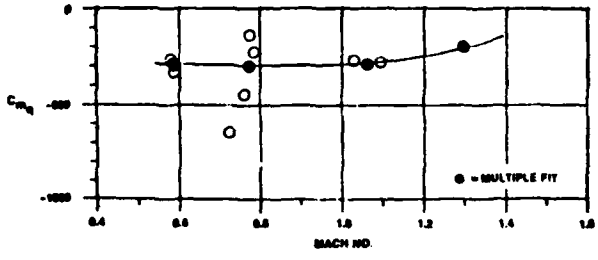

Figure 8. Damping-In-Pitch Derivatives

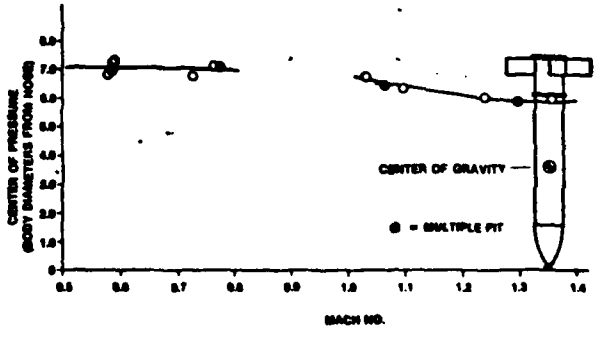

Figure 9. Location of the Center of Pressure

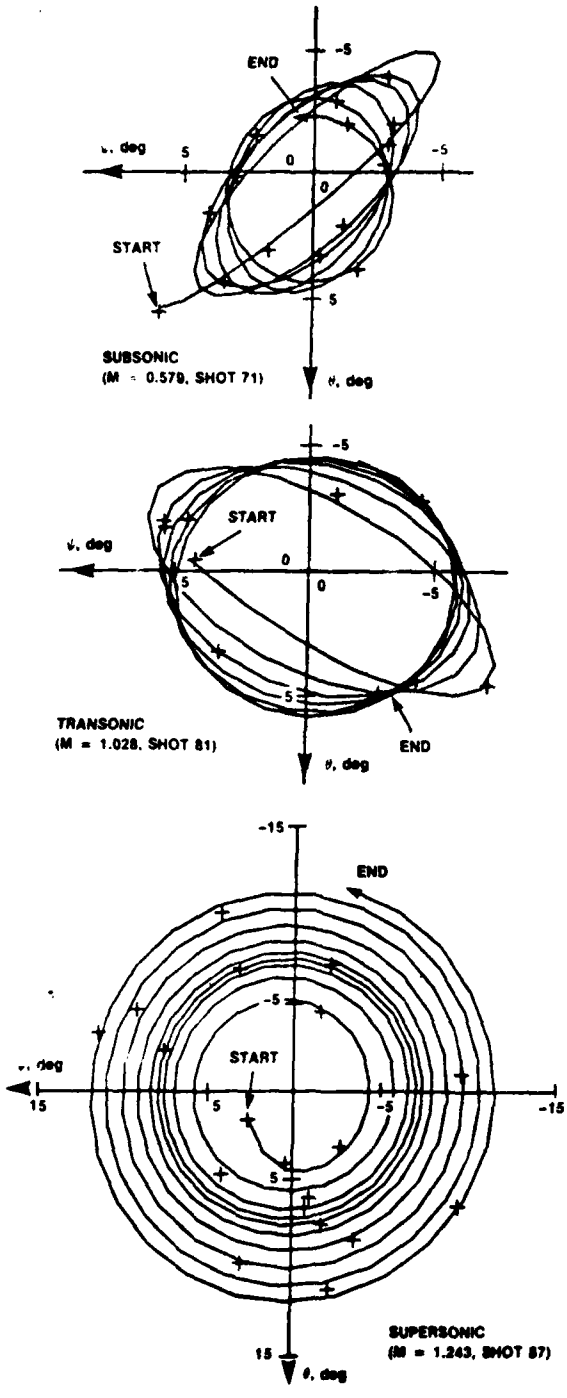

Figure 11. Typical Angular Motion Plots

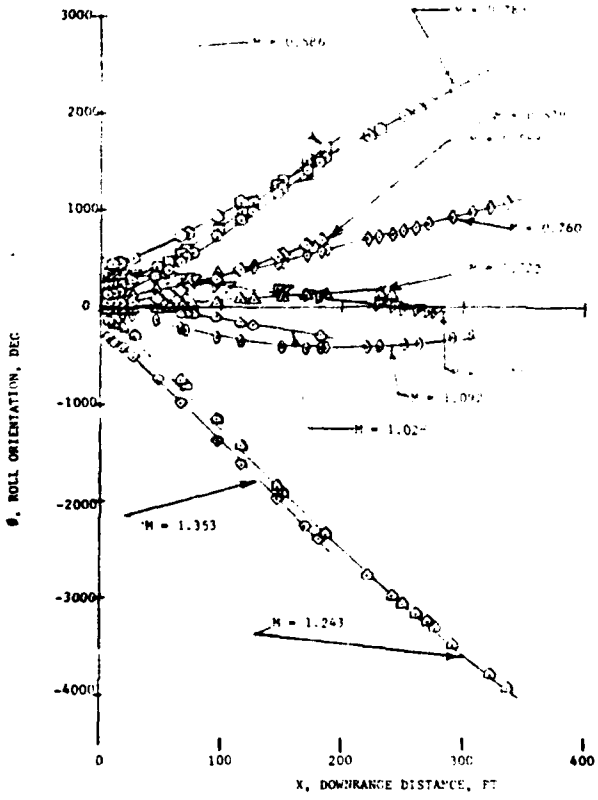

Figure 12. Measured and Fitted Roll Profiles

Discussion

Initially it was suspected that the motion growth problem at supersonic Mach numbers, as shown in Figure 11, was caused by a classic pitch-roll resonance. This is particularly true since the damping-in-pitch derivatives were negative, (see Figure 8) and the models displayed unusual roll characteristics, as described in the previous section. Also the linear theory results, shown in Table 3, indicate that the supersonic flights, shots 87 and 88, were near resonance ($\frac{p}{\omega_n} \cong 1$).

The motion growth caused by the resonant condition is due to an increase in the magnitude of the trim vector (K_T).[10, 12] This increase in the magnitude of the trim vector is graphically portrayed in the sketch of Figure 13 and shows that

$$/ K_T / _{res} = (\text{amplification factor}) \cdot / K_T / _{p=0} \quad (19)$$

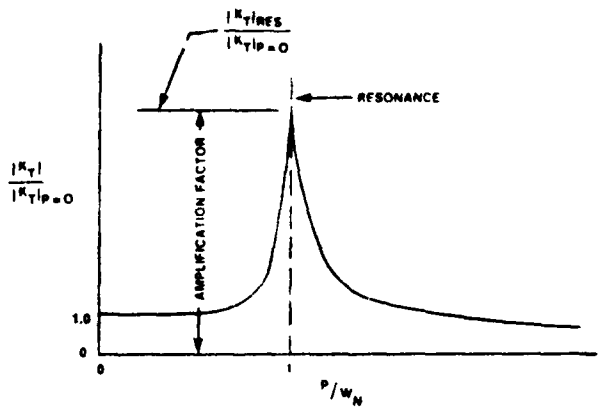

Figure 13. Typical Aerodynamic Trim as a Function of Spin Rate

Once the aerodynamic coefficients and derivatives have been determined for a particular configuration, the Amplification Factor (AF) can be approximated using the following relation[12]:

$$AF \cong \frac{-\frac{\bar{m}d}{I_y \omega_{10}} C_{m\alpha}}{C_{N\alpha} - \frac{\bar{m}d^2}{2 I_y}(C_{mq})} \qquad (20)$$

Thus, substituting in the measured physical properties of the models (Table 1) the determined aerodynamics (Figures 5 through 10), the Amplification Factor (AF) associated with the supersonic flights (M ≅ 1.23, shots 87 and 88) was computed to be about 12. Since these two flights were near resonance, it would therefore be expected that the trim vectors associated with these flights had increased to be no more than 12 times larger than the zero spin trim case. However, the 6DOF analysis indicated that the zero spin trim vectors were small, less than 0.25 degree. In fact, the trim vectors were so small that linear theory could not determine the magnitude of K_T, and they were assumed to be zero (see Table 3). Therefore, the motion growth related to the resonance condition would be expected to be less than 3 degrees. This obviously does not account for the motion growth, shown in Figure 11, for the supersonic flight of shot 87, and the cause of this dynamic instability must be found elsewhere.

The only other unconventional ~~aspet~~ aspect of the 6DOF analysis was the addition of the side moment derivative due to pitch. As was previously discussed, this derivative, ($C_{n\alpha}$), was included in the moment equations in order to adequately fit the measured motion patterns. The question then becomes: can this side moment be causing the dynamic instability problems at the supersonic conditions? The tendency of the motion to develop into a circular pattern (as mentioned in the previous section) provides a clue into the possible effects of this side moment. Both Murphy[10] and Nicolaides[12] have studied the consequences of a side moment due to pitch on the dynamic stability of a finned missile. The equations for the computation of the nutational and precessional damping rates, as expressed by Nicolaides[12], including $C_{n\alpha}$, are shown as follows:

$$\lambda_1 = \frac{\rho A}{4\bar{m}}\left[-C_{N\alpha}\left(1 - \frac{1}{\sigma}\right) + (C_{mq} + C_{m\dot{\alpha}})\left(\frac{\bar{m}d^2}{2I_y}\right)\left(1 + \frac{1}{\sigma}\right) + \frac{\bar{m}d^2}{I_x}\left(\frac{1}{\sigma}\right) C_{n\alpha}\left(\frac{2V}{pd}\right)\right] \qquad (21)$$

$$\lambda_2 = \frac{\rho A}{4\bar{m}}\left[-C_{N\alpha}\left(1 + \frac{1}{\sigma}\right) + (C_{mq} + C_{m\dot{\alpha}})\left(\frac{\bar{m}d^2}{2I_y}\right)\left(1 - \frac{1}{\sigma}\right) - \frac{\bar{m}d^2}{I_x}\left(\frac{1}{\sigma}\right) C_{n\alpha}\left(\frac{2V}{pd}\right)\right] \qquad (22)$$

where

$$\sigma = \sqrt{1 - \frac{I}{S_g}} \qquad (23)$$

and

$$S_g = \frac{2 I_x^2 p^2}{\pi \rho I_y C_{m\alpha} d^3 V^2} \qquad (24)$$

Equations (21) and (22) assume that the Magnus moment is negligible and, substituting in the measured physical properties and the determined aerodynamic derivatives at the test Mach numbers, the associated damping rates were computed. These computations are listed in Table 4 for various values of $C_{n\alpha}$ and spin. As is shown for Mach 0.57, the damping rates, (λ_1 and λ_2), were insensitive to variations in the spin rate (p), from near zero to resonance. However, variations in the side moment derivative, ($C_{n\alpha}$), from -1 to -5 significantly altered the computed damping rates. Since the damping rates were shown to be insensitive to spin at Mach 0.59, the computations for Mach numbers of 0.77, 1.06, and 1.30 used a spin rate of about one-half resonance. The computed λ_2 values show that as $C_{n\alpha}$ is varied from -1 to -5, this damping rate tends to become positive (undamped). Also this undamping trend appears to get more severe as the Mach number increases. In fact, at Mach 1.3 a $C_{n\alpha}$ value of -3 causes an undamped λ_2. It should be noted that this value of -3 for $C_{n\alpha}$ at Mach 1.3 is about what $C_{n\alpha}$ was determined to be from the 6DOF analysis (see Figure 10). Also the trends in the computed λ_2 values shown in Table 4 agree well with the measured linear theory values listed in Table 3. It was therefore concluded that this side moment, which appears to be symptomatic of WAF configurations, is the cause of the dynamic instability as measured at the supersonic condition.

The stability boundaries can also be determined by setting λ_2 equal to zero in equation (22) and solving for $C_{n\alpha}$. These stability boundaries are shown in Figure 14 along with the determined slopes of C_m and C_n for each of the test Mach numbers. This figure confirms that subsonically the determined side moments fall in the dynamically stable region; whereas, supersonically, the side moments are dynamically destabilizing. This figure also indicates that the stable region is decreasing with Mach number; or, that very small values of $C_{n\alpha}$ can cause a dynamic instability at Mach 1.3.

Table 4. DYNAMIC STABILITY COMPUTATIONS

MACH	C_{N_α}	C_{m_α}	C_{m_q}	C_{n_α}	P (RAD/SEC)	λ_1 (1/m)	λ_2 (1/m)
0.59	14.0	-46.0	-288	-1.0	0.1	-0.0366	-0.0216
0.59	14.0	-46.0	-288	-1.0	70.2	-0.0367	-0.0215
0.59	14.0	-46.0	-288	-1.0	140.4	-0.0367	-0.0214
0.59	14.0	-46.0	-288	-3.0	0.1	-0.0516	-0.0065
0.59	14.0	-46.0	-288	-3.0	70.2	-0.0517	-0.0065
0.59	14.0	-46.0	-288	-3.0	140.4	-0.0518	-0.0064
0.59	14.0	-46.0	-288	-5.0	0.1	-0.0666	+0.0085
0.59	14.0	-46.0	-288	-5.0	70.2	-0.0667	+0.0086
0.59	14.0	-46.0	-288	-5.0	140.4	-0.0668	+0.0087
0.77	15.0	-52.0	-300	-1.0	93.5	-0.0377	-0.0234
0.77	15.0	-52.0	-300	-3.0	93.5	-0.0519	-0.0093
0.77	15.0	-52.0	-300	-5.0	93.5	-0.0660	+0.0048
1.06	14.6	-41.0	-290	-1.0	128.7	-0.0377	-0.0216
1.06	14.6	-41.0	-290	-3.0	128.7	-0.0536	-0.0057
1.06	14.6	-41.0	-290	-5.0	128.7	-0.0695	+0.0102
1.30	14.0	-32.0	-200	-1.0	152.0	-0.0323	-0.0142
1.30	14.0	-32.0	-200	-3.0	152.0	-0.0503	+0.0038
1.30	14.0	-32.0	-200	-5.0	152.0	-0.0683	+0.0218

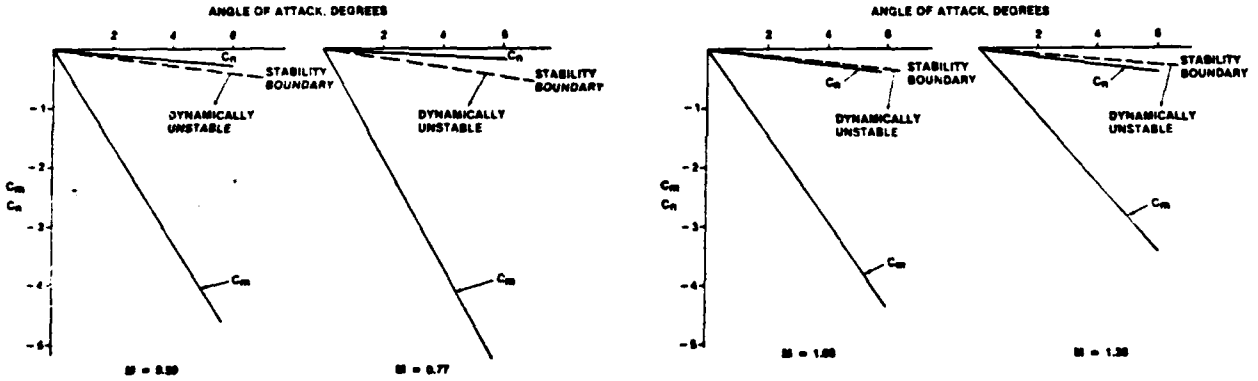

Figure 14. Dynamic Stability Boundary Conditions

Conclusions

The results of a free flight range test of a WAF configuration at subsonic and transonic Mach numbers indicated that an out-of-plane side moment due to pitch angle was prevalent. This side moment caused a dynamic instability at the supersonic Mach numbers. Linear theory accurately predicts this dynamic instability assuming that the side moment has been measured. It is suspected that this side moment is symptomatic of WAF configurations; when testing such configurations, the test engineer should ensure that this side moment is obtained and the stability boundaries are computed. Designers of such configurations should also consider the possibility of this side moment because it can have a dramatic effect on trajectory computations based on the conventional aerodynamic coefficients and derivatives.

References

1. Dahlke, C.W. and Flowers, L.D. "The Aerodynamic Characteristics of Wraparound Fins, Including Fold Angle at Mach Numbers From 0.5 to 1.3.," U.S. Army Missile Command, Redstone Arsenal, Alabama, TR-RD-75-19, 20 December, 1974.

2. Humphrey, James A. and Dahlke, Calvin W. "A Summary of Aerodynamic Characteristics For Wraparound Fins from Mach 0.3 to 3.0," U.S. Army Missile Research and Development Command, Redstone Arsenal, Alabama, TR-TD-77-5, March, 1977.

3. Pope, R.L. and Dudley, E.E. "Flight Tests of the MK IV Wraparound Fin Configuration, "Weapons Systems Research Laboratory, Defense Research Center, Salisbury, South Australia, WSRL-0252 TR, January, 1982.

4. Dahlke, C.W. and Craft, J.C. "The Effect of Wraparound Fins on Aerodynamic Stability and Rolling Moment Variations," U.S. Army Missile Command, Redstone Arsenal, Alabama, TR-RD-17, July, 1973.

5. Hardy, Samuel R. "Nonlinear Analysis of the Rolling Motion of a Wraparound Fin Missile at Angles of Attack from 0 to 90 Degrees in Incompressible Flow," Naval Surface Weapons Center, Dahlgren, Virginia, NSWCDL-TR-3727, September, 1977.

6. Cohen, C.J., Clare, T.A., and Steens, F.L. "Analysis of the Nonlinear Rolling Motion of Finned Missile," AIAA paper No. 72-980, Palo Alto, CA, 1972.

7. Winchenbach, G., Galanos, D., Kleist, J., and Lucas, B., "Description and capabilities of the Aeroballistic Research Facility," AFATL-TR-78-41, February 1978.

8. Whyte, R.H., Winchenbach, G., and Hathaway, W.H., "Subsonic Free Flight Data for a Complex Asymmetric Missile," Journal of Guidance and Control, Vol. 4, Number 1, January-February 1981, pg 59-65.

9. Murphy, C.H., "Data Reduction for the Free Flight Spark Ranges," BRL-Report 900, February 1954.

10. Murphy, C.H., "Free Flight Motion of Symmetric Missile," BRL-Report 1216, July 1963.

11. Winchenbach, G.L., Uselton, R.L., Hathaway, W.H., and Chelekis, R.M., "Free Flight and Wind Tunnel Data for a Generic Fighter Configuration," Journal of Aircraft, Vol. 21, Number 1, January 1984. pp 5-13.

12. Nicolaides, J.D., "Free Flight Dynamics," University of Notre Dame, 1968.

END

FILMED

7-85

DTIC